23PM1P-26

Analysis of the Electromagnetic Field Scattered by a Spherical Breast Tumour Model

İlhami Ünal [#1], Bahattin Turetken [*2], Umut Bulus [*3], Cahit Canbay [#4]

[#] *Department of Electrical and Electronics Engineering, Yeditepe University*
26 Ağustos Yerleşimi, 34755, Kayışdağı, İstanbul, Turkey
[1] ilhamiunal@yeditepe.edu.tr
[4] canbay@yeditepe.edu.tr

[*] *Antenna Test and Research Center (ATAM), TUBITAK – BILGEM – UEKAE*
PO 74, Gebze, Kocaeli, Turkey
[2] bahattin.turetken@tubitak.gov.tr
[3] umut.bulus@tubitak.gov.tr

***Abstract*—In this paper, a closed form solution is presented for the electromagnetic field scattered due to a lossy dielectric spherical tumour with arbitrary diameter, inside a lossy dielectric breast fat tissue medium. The analytical and simulation results are successfully compared to each other. Using this analytical method, we demonstrate the importance of accounting for selection of polarization and operation frequency of antennas used in a microwave imaging system for breast cancer tumour detection.**

I. INTRODUCTION

Early diagnosis and treatment are the hot keys to survive from breast cancer. The present standard screening technology for detecting breast cancer is X-ray mammography. It has several limitations, especially when dealing with younger women who have dense breast tissues. It requires painful and uncomfortable breast compression and exposes the patient to ionizing radiation.

Electromagnetic waves and antennas have a huge application area, and one of the challenging areas is remote sensing systems and detection systems using microwaves, today. There are various passive and active microwave techniques which have been proposed as an alternative especially to the most widely used X-ray mammography for early detection of breast cancer, such as microwave radiometry [1], hybrid microwave-induced acoustic imaging [2], microwave tomography [3] and UWB microwave radar technique [4], [5].

The passive methods (microwave radiometry) use radiometers to measure the temperature differences in the breast as temperature increases in the presence of tumour than with healthy breast tissue. The hybrid methods (microwave-induced acoustic imaging) use microwave energy to heat tumours. They expand and generate pressure waves which are detected by ultrasound transducers. In microwave tomography, an inverse scattering problem is solved to reconstruct an image of the dielectric properties in the breast. In contrast to the image reconstruction aim of the microwave tomography technique, UWB radar-based imaging approach solves a simpler computational problem faster dealing with only to identify the presence and location of significant scattering obstacles such malignant breast tumours.

There is a significant contrast in the electrical properties of the normal and the malignant breast tissues [4], which exists in the earliest stage of tumour development, at microwave frequencies. Another advantage of the microwave imaging technique is that it would be nonionizing and it doesn't require painful breast compression. Furthermore, microwave attenuation in normal breast tissue is low enough to make signal propagation through even large breast volumes quite feasible [4]. Other available screening techniques such as ultrasound and MRI are either less effective or are too costly.

In this study, we're interested in the 1–8 GHz frequency range; which has a balance between resonable contradictory needs of better spatial resolution and better penetration depth [6], for microwave imaging applications. In order to obtain the information about the existence and position of the malignant tumour, it is important to understand the electromagnetic scattering phenomenon of the tumour. Previously, cylindrically and spherically shaped tumour models have been presented to estimate the electromagnetic scattering features [7]-[12]. In one of the most recent analytical studies [11], the tumour was considered to have dimensions which were significantly smaller than the used wavelength assuming the case of an early stage cancer. In this paper, the previous methods of scattering analysis is extended to investigate the electromagnetic scattering from a lossy and dispersive dielectric spherical tumour with arbitrary diameter (in the 1-8 GHz frequency range) inside a lossy and dispersive dielectric breast fat tissue by using spherical vector wave functions. The dependence of the scattered field pattern on the tumour diameter and frequency, as well as polarization features of scattered fields are all presented. Comparable results of the scattered fields by the tumour inside breast fat and fibro-glandular tissues are also discussed.

II. ANALYTICAL STUDY

For a plane wave incident in positive z-axis direction (see Fig. 1), incident electric and magnetic fields can be expressed as:

$$\vec{E}^i = E_0\, e^{-jkz}\, \vec{a}_x$$
$$\vec{H}^i = \vec{H}_0\, e^{-jkz}\, \vec{a}_y \tag{1}$$

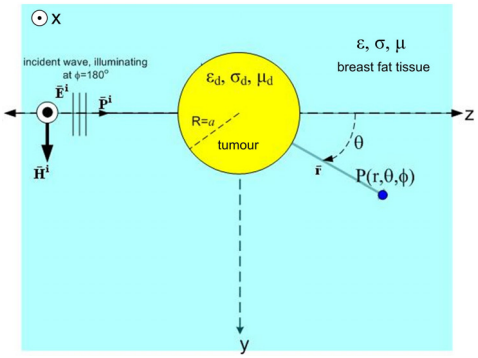

Fig. 1. Illustration of an incident electromagnetic wave on a lossy and dispersive dielectric tumour inside a lossy and dispersive breast fat tissue.

The vector potentials can be written as,

$$\vec{A} = A_r\, \vec{a}_r$$
$$\vec{F} = F_r\, \vec{a}_r \tag{2}$$

$\vec{A}$ and $\vec{F}$ produce TM and TE (with respect to *r*) mode fields, respectively. The sum of the incident and scattered magnetic and electric vector potentials can be expanded as series [13]:

$$A_r^+ = \frac{E_0}{\omega\mu}\cos(\phi) \times \sum_{n=1}^{\infty}\left[a_n \hat{J}_n(kr) + b_n \hat{H}_n^{(2)}(kr)\right]P_n^1(\cos(\theta))$$
$$F_r^+ = \frac{E_0}{k}\sin(\phi) \times \sum_{n=1}^{\infty}\left[a_n \hat{J}_n(kr) + c_n \hat{H}_n^{(2)}(kr)\right]P_n^1(\cos(\theta)) \tag{3}$$

for outside the spherical tumour (*r*>*a*), and

$$A_r^- = \frac{E_0}{\omega\mu}\cos(\phi)\sum_{n=1}^{\infty} d_n \hat{J}_n(k_d r)P_n^1(\cos(\theta))$$
$$F_r^- = \frac{E_0}{k}\sin(\phi)\sum_{n=1}^{\infty} e_n \hat{J}_n(k_d r)P_n^1(\cos(\theta)) \tag{4}$$

for inside the spherical tumour (*r*<*a*),

where $\hat{J}_n(kr) = kr\, j_n(kr)$, $\hat{H}_n^{(2)}(kr) = kr\, h_n^{(2)}(kr)$,

$P_n^1(\cos(\theta)) = \dfrac{\partial P_n(\cos(\theta))}{\partial\theta}$, $a_n = \dfrac{j^{-n}(2n+1)}{n(n+1)}$,

$k = \sqrt{\omega^2\varepsilon\mu - j\sigma\omega\mu}$, $k_d = \sqrt{\omega^2\varepsilon_d\mu_d - j\sigma_d\omega\mu_d}$.

With the continuity of $E_\theta^+ = E_\theta^-$, $E_\phi^+ = E_\phi^-$, $H_\theta^+ = H_\theta^-$, and $H_\phi^+ = H_\phi^-$ at *r*=*a*, one can obtain the closed form equations of the unknown constants; b_n, c_n, d_n and e_n, as follows:

$$b_n = a_n \frac{\xi\hat{J}_n'(ka)\hat{J}_n(k_d a) - \xi_d \hat{J}_n(ka)\hat{J}_n'(k_d a)}{\xi_d \hat{H}_n^{(2)}(ka)\hat{J}_n'(k_d a) - \xi\hat{H}_n^{(2)\prime}(ka)\hat{J}_n(k_d a)} \tag{5}$$

$$c_n = a_n \frac{k\mu_d \hat{J}_n(k_d a)\hat{J}_n'(ka) - k_d\mu\hat{J}_n'(k_d a)\hat{J}_n(ka)}{k_d\mu\hat{J}_n'(k_d a)\hat{H}_n^{(2)}(ka) - k\mu_d\hat{J}_n(k_d a)\hat{H}_n^{(2)\prime}(ka)} \tag{6}$$

$$d_n = a_n \frac{\xi\hat{H}_n^{(2)\prime}(ka)\hat{J}_n(ka) - \xi\hat{H}_n^{(2)}(ka)\hat{J}_n'(ka)}{\xi\hat{H}_n^{(2)\prime}(ka)\hat{J}_n(k_d a) - \xi_d\hat{H}_n^{(2)}(ka)\hat{J}_n'(k_d a)} \tag{7}$$

$$e_n = a_n \frac{k\mu_d \hat{H}_n^{(2)\prime}(ka)\hat{J}_n(ka) - k_d\mu\hat{H}_n^{(2)}(ka)\hat{J}_n'(ka)}{k\mu_d\hat{H}_n^{(2)\prime}(ka)\hat{J}_n(k_d a) - k_d\mu\hat{H}_n^{(2)}(ka)\hat{J}_n'(k_d a)} \tag{8}$$

where $\xi = k/(\sigma + j\omega\varepsilon)$ and $\xi_d = k_d/(\sigma_d + j\omega\varepsilon_d)$.

The resulting scattering field components are as follows:

$$E_{rs} = \frac{E_0 k\xi}{\omega\mu}\cos(\phi)\left[\sum_{n=1}^{\infty} b_n \hat{H}_n^{(2)}(kr)P_n^1(\cos(\theta))\right] + \frac{E_0 k\xi}{\omega\mu}\cos(\phi)\left(\sum_{n=1}^{\infty} b_n \hat{H}_n^{(2)\prime\prime}(kr)P_n^1(\cos(\theta))\right) \tag{9}$$

$$E_{\theta s} = -\frac{E_0}{kr}\cos(\phi)\frac{1}{\sin(\theta)}\left[\sum_{n=1}^{\infty}\left[c_n \hat{H}_n^{(2)}(kr)\right]P_n^1(\cos(\theta))\right] + \frac{-E_0\xi}{r\omega\mu}\cos(\phi)\sin(\theta)\left(\sum_{n=1}^{\infty} b_n \hat{H}_n^{(2)\prime}(kr)P_n^{1\prime}(\cos(\theta))\right) \tag{10}$$

$$E_{\phi s} = \frac{-E_0\sin(\theta)\sin(\phi)}{kr}\left[\sum_{n=1}^{\infty}\left[c_n \hat{H}_n^{(2)}(kr)\right]P_n^{1\prime}(\cos(\theta))\right] + \frac{-E_0\xi}{r\omega\mu\sin(\theta)}\sin(\phi)\left(\sum_{n=1}^{\infty} b_n \hat{H}_n^{(2)\prime}(kr)P_n^1(\cos(\theta))\right) \tag{11}$$

III. NUMERICAL RESULTS AND DISCUSSIONS

In order to validate the accuracy of the analytical derivations, a full-wave electromagnetic solver FEKO is used for simulations. To include the frequency dependence of dielectric properties of the breast fat, tumour and fibro-glandular tissues, the first Debye dispersion model has been applied assuming the values such as ε_∞, ε_s and σ_s, as in [9], [14] valid from 100 MHz to 20 GHz and shown in Table 1:

$$\varepsilon_r = \varepsilon_\infty + \frac{\varepsilon_s - \varepsilon_\infty}{1 + j\omega\tau} - j\frac{\sigma_s}{\omega\varepsilon_0} \tag{12}$$

where ε_s is the relative low-frequency permittivity, ε_∞ is the relative high-frequency permittivity, τ is the relaxation time, ε_0 is the permittivity of free-space, and ω is the angular frequency and σ_s is the ionic conductivity.

TABLE I
DEBYE MODEL PARAMETERS

Tissue	ε_∞	ε_s	τ (ps)	σ_s (S/m)
Breast Fat [9]	7	10	7	0.15
Tumour [9]	4	54	7	0.70
Fibro-glandular [14]	12.84	37.49	13	0.25

The analytical and simulation (FEKO) results of amplitude and phase of the scattered field ($E_{\phi s}$) with respect to θ are successfully compared to each other, as shown Fig. 1 and Fig. 2, respectively. The magnetic permeability of both breast fat and tumour are taken as ($\mu_d = \mu = \mu_0 = 4 \cdot \pi \cdot 10^{-7} \left(H/m \right)$), which is the common case. E_0 is taken as 1 V/m and radial measurement distance r is taken as 30 mm for all calculations and simulations, which are taken on y-z plane with $\phi=\pi/2$.

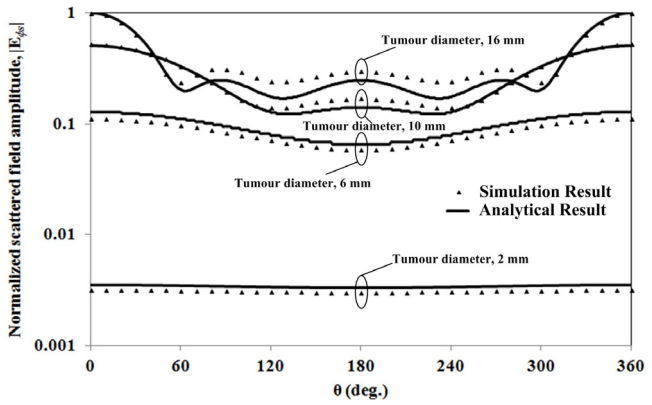

Fig. 2. Normalized scattered field amplitude, $\left|E_{\phi s}\right|$ with respect to θ, for different diameters of spherical tumour models

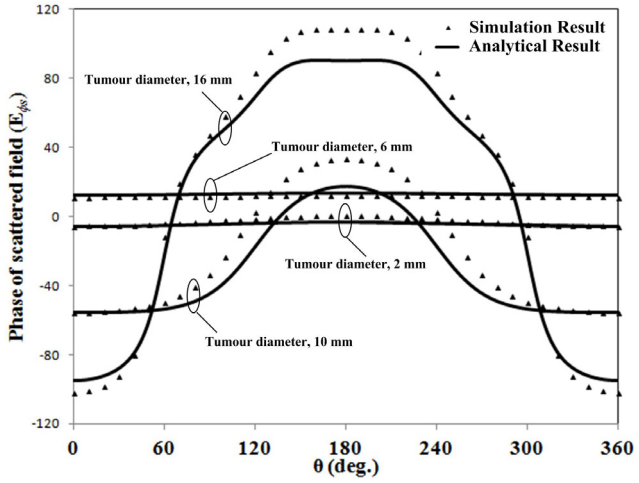

Fig. 2. Phase of scattered field, $E_{\phi s}$ with respect to θ, for different diameters of spherical tumour models

If one investigates the scattered field pattern with respect to θ for different operation frequencies, for tumour diameters of both 2 mm and 10 mm (see Fig. 3 and Fig. 4), it's observed that the scattered field pattern is almost uniformly distributed around the tumour for low frequencies. As the operation frequency increases, the back-scattered fields become highly dependent on θ. On the other hand, the scattered fields are generally greater for bigger tumours, especially at $\theta = 0^o$.

The back-scattered field amplitude with respect to different operation frequencies (1-8 GHz) has been also investigated for tumours with different diameters, as shown in Fig. 5. As the operation frequency increases, the back-scattered fields also increase at $\theta = 180^o$. As it's expected, the value of the back-scattered field for small tumours increases approximately with the square of the frequency, [10].

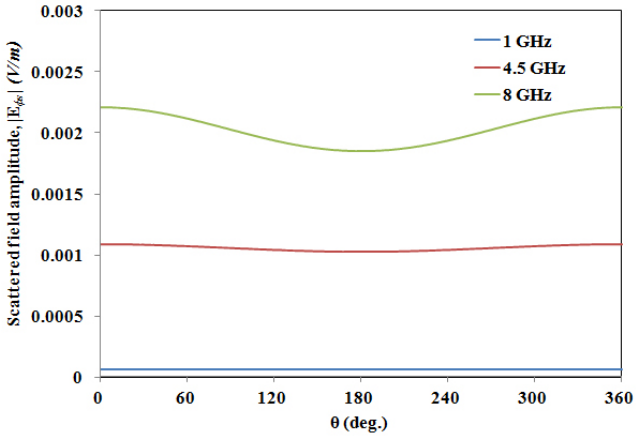

Fig. 3. Scattered field amplitude, $\left|E_{\phi s}\right|$ with respect to θ, for different operation frequencies for tumour diameter of 2 mm

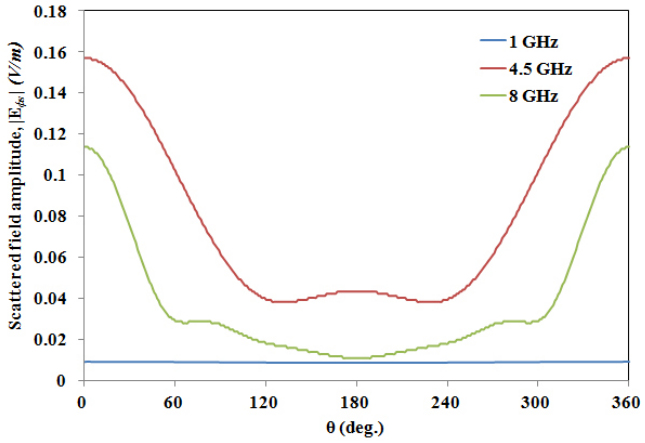

Fig. 4. Scattered field amplitude, $\left|E_{\phi s}\right|$ with respect to θ, for different operation frequencies for tumour diameter of 10 mm

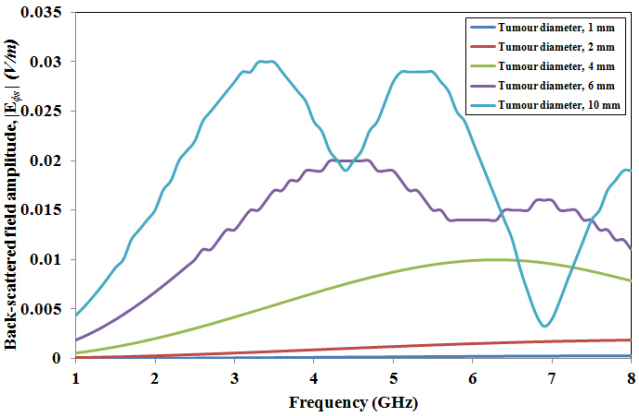

Fig. 5. Scattered field amplitude, $\left|E_{\phi s}\right|$ with respect to θ, for different operation frequencies for tumour diameter of 10 mm

For bigger tumours, oscillations in Fig. 5 correspond to the resonance region between Rayleigh and optical approximations [13]. On the other hand, expected increment of the scattered fields by especially small tumours with frequency may have a positive impact on the dynamic range of an UWB microwave imaging system as the propagation loss of the incident and scattered field increases with the frequency [10].

If we compare the scattered field pattern results of tumour with 8 mm diameter inside breast fat and fibro-glandular tissues, the scattered field level is decreased for the tumour inside the fibro-glandular tissues; because of higher permittivity and conductivity values of the fibro-glandular tissue.

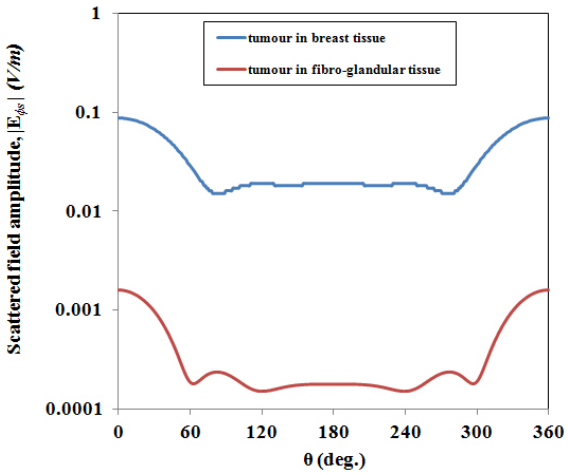

Fig. 6. Comparison of scattered field by the tumour with 8 mm diameter inside breast fat and fibro-glandular tissues

The scattered fields have all of the three r, θ and ϕ-components, as in (9)-(11). However, in this study only ϕ-component of the scattered field has been analysed because other cross-polarized θ and r-components of the scattered field have negligible values compared to the co-polarized one, in y-z plane. Some of the researchers tried to use the co- and cross-polarized scattered fields to estimate the existence of the tumour [15]. However, the cross-polarized scattered field components seem to have a very low value. On the other hand, one should also investigate the scattering properties of the tumour inside a more realistic heterogeneous breast model from polarization point of view. It would helpful to design perfectly polarized antennas to the tumour, for increasing dynamic range of a microwave imaging system.

IV. Conclusion

In this study, a closed form analytical solution has been presented for the electromagnetic field scattered due to a lossy dielectric spherical tumour with arbitrary diameter, inside a lossy dielectric breast fat tissue medium. Based on the knowledge of the possible distribution and polarization of those scattered fields around the tumour, electromagnetic scattering features of the tumour should also be taken into account for the design of a probe antenna to improve the tumour detection capability of a microwave imaging system. Analyses of the study can also be extended for observing three-dimensional scattering properties of the spherical tumour, in the future.

References

[1] K. L. Carr, "Microwave radiometry: Its importance to the detection of cancer," *IEEE Trans. Microwave Theory and Tech.*, vol. 37, pp. 1862–1869, Dec. 1989.

[2] L. V. Wang, X. Zhao, H. Sun, and G. Ku, "Microwave-induced acoustic imaging for biological tissues," *Rev. Sci. Instrum.*, vol. 70, pp. 3744–3748, Sep. 1999.

[3] A. E. Bulyshev, S. Y. Semenov, A. E. Souvorov, R. H. Svenson, A. G. Nazarov, Y. E. Sizov, and G. P. Tatsis, "Computational modelling of three-dimensional microwave tomography of breast cancer," *IEEE Trans. Biomed. Eng.*, vol. 48, pp. 1053–1056, Sep. 2001.

[4] E. C. Fear, X. Li, S. C. Hagness, and M. A. Stuchly, "Confocal microwave imaging for breast tumor detection: Localization in three dimensions," *IEEE Trans. Antennas Propag.*, vol. 49, pp. 812–822, Aug. 2002.

[5] M. Klemm, J. A. Leendertz, D. Gibbins, I. J. Craddock, A. Preece, and R. Benjamin, "Microwave radar-based differential breast cancer imaging: Imaging in homogeneous breast phantoms and low contrast scenarios," *IEEE Trans. Antennas Propag.*, vol. 58, pp. 2337–2344, July 2010.

[6] N. Tavassolian, S. Nikolaou, and M. M. Tentzeris, "A flexible UWB elliptical slot antenna with a tuning uneven U-shape stub on LCP for microwave tumor detection," in *Asia-Pasific Microwave Conference*, 2007, 1-4.

[7] Z. Q. Zhang, Q. H. Liu, C. Xiao, E. Ward, G. Ybarra, and W. T. Joines, "Microwave breast imaging: 3-D forward scattering simulation," *IEEE Trans. Biomed. Eng.*, vol. 50, pp. 1180–1189, Oct. 2003.

[8] G. G. Senaratne, R. B. Keam, W. L. Sweatman, and G. C. Wake "Microwave scattering at malignant tissue boundaries: A new method for breast screening," in *SICE-ICASE*, 2006, pp. 193-197.

[9] A. M. Abbosh, M. E. Bialkowski, and S. Crozier, "Investigations into optimum characteristics for the coupling medium in UWB breast cancer imaging systems," in *IEEE Antennas and Propagation Symp.*, 2008.

[10] A. M. Abbosh, M. E. Bialkowski, and S. Crozier, "A simple model for electromagnetic scattering due to breast tumour," in *IEEE Antennas and Propagation Symp.*, 2008.

[11] A. M. Abbosh and A. A. Bakar, "Three-dimensional modeling of electromagnetic scattering from breast tumor," in *Proc. Asia-Pacific Microwave Conference*, 2010, pp. 1384-1387.

[12] N.A. Simonov, S. I. Jeon, S. H. Son, J. M. Lee, and H. J. Kim "Modeling signals of small tumors inside the breast in ultra-wide frequency band," in *Proc. 5th European Conference on Antennas and Propagation*, 2011, pp. 493-497.

[13] R. F. Harrington, *Time-Harmonic Electromagnetic Fields*, 2nd ed., D. G. Dudley, Ed. Wiley-IEEE Press, 2001.

[14] E. Zastrow, S. K. Davis, M. Lazebnik, F. Kelcz, B. D. Van Veen, and S. C. Hagness, "Development of anatomically realistic numerical breast phantoms with accurate dielectric properties for modeling microwave intereactions with the human breast," *IEEE Trans. Biomed. Eng.*, vol. 55, pp. 2792–2800, Dec. 2008.

[15] S. C. Hagness, A. Taflove, and J. Bridges, "Three dimensional FDTD analysis of a pulsed microwave confocal system for breast cancer detection," *IEEE Trans. Antennas. Propag.*, vol. 47, pp. 783–791, May 1999.